

RSC Advances



This is an *Accepted Manuscript*, which has been through the Royal Society of Chemistry peer review process and has been accepted for publication.

Accepted Manuscripts are published online shortly after acceptance, before technical editing, formatting and proof reading. Using this free service, authors can make their results available to the community, in citable form, before we publish the edited article. This *Accepted Manuscript* will be replaced by the edited, formatted and paginated article as soon as this is available.

You can find more information about *Accepted Manuscripts* in the [Information for Authors](#).

Please note that technical editing may introduce minor changes to the text and/or graphics, which may alter content. The journal's standard [Terms & Conditions](#) and the [Ethical guidelines](#) still apply. In no event shall the Royal Society of Chemistry be held responsible for any errors or omissions in this *Accepted Manuscript* or any consequences arising from the use of any information it contains.

Studies on Structural, Thermal, Optical, Electrical and Nanomechanical Properties of Sputtered Vanadium Oxide Smart Thin Films

Deeksha Porwal^{1,3**}, Carmel Mary Esther A^{1**}, I. Neelakanta Reddy², N. Sridhara¹, Nagendra Prasad Yadav³, Dinesh Rangappa⁴, Parthasarathi Bera⁵, Chinnasamy Anandan⁵, Anand Kumar Sharma¹ and Arjun Dey^{1*}

¹Thermal System Group, ISRO Satellite Centre, Bangalore 560017, India

²Centre for Nanoscience and Nanotechnology, Sathyabama University, Chennai 600119, India

³Bundelkhand Institute of Engineering and Technology, Jhansi 284128, India

⁴Center for Nanotechnology, Center for Post Graduate studies, Visvesvaraya Technological University, Belgaum 590018, India

⁵Surface Engineering Division, CSIR–National Aerospace Laboratories, Bangalore 560017, India

Abstract

Vanadium oxide thin films were grown on both quartz and Si(111) substrates utilizing pulsed RF magnetron sputtering technique at room temperature with RF power at 100 W to 700 W. The corresponding thicknesses of the films were increased from 27.5 nm to 243 nm and 21 nm to 211 nm as RF power increased from 100 W to 700 W for quartz and silicon substrates, respectively. X-ray diffraction and field emission scanning electron microscopy were carried out to investigate the phase and surface morphology of the deposited films. Electronic structure and vanadium oxidation states of the deposited films were investigated thoroughly by X-ray photoelectron spectroscopy. As-grown films show stoichiometric vanadium oxide only where vanadium is in V⁵⁺ and V⁴⁺ states. Phase transition of vanadium oxide films were investigated by differential scanning calorimetric technique. The reversible i.e. smart transition was observed in the region from 337 °C to 343 °C. Average hemispherical emittance of the deposited vanadium oxide films was evaluated by an emissometer in the wavelength range of 3 μm to 30 μm. The sheet resistance of the deposited films was measured by two-probe method and data were in the range of 10⁶ to 10⁵ Ω/square. Optical properties of the films such as solar transmittance, solar reflectance and solar absorptance as well as optical constants e.g. optical band gap were also evaluated. Finally, mechanical properties such as nanohardness and Young's modulus at microstructural length scale were evaluated employing nanoindentation technique with continuous stiffness mode.

Keywords: Vanadium oxide; Thin film; Phase transition; Thermo-optical properties; Nanoindentation; Sheet resistance.

*Corresponding author. Tel.: +91 80 2508 3214; fax: +91 80 2508 3203.

E-mail addresses: arjundey@isac.gov.in, arjun_dey@rediffmail.com (A. Dey).

**Both authors worked equally

1. Introduction

Vanadium oxide shows a drastic reversible change in solar transmittance, infrared (IR) emittance and electrical resistance with alteration in either temperature (i.e., thermochromic behaviour) or potential difference (i.e., electrochromic behaviour). This reversible change in properties occurs primarily due to metal-to-insulator transition (MIT) and was first reported by Mott^{1,2} which is commonly referred as smart transition. According to Mott^{1,2}, vanadium oxide undergoes reversible change in crystal structure (i.e., insulator to metallic state) which leads to change in energy band gap while increase and subsequently decrease in temperature above or below in its transition point. Now, at the transition point, a lattice distortion takes place in vanadium oxide and thereby leads to energy gap separation from empty state. Further, increase in temperature gives diminishing of lattice distortion due to excitation of electrons which results reduction in energy gap and hence it acts as metallic state.

Among all oxides of vanadium, VO₂ and V₂O₅ possess the phase transition in positive temperature range while the remaining oxides show the transition at sub-zero temperature range³. Due to this, VO₂ and V₂O₅ are well studied in literature in comparison with the other oxides of vanadium mentioned above^{3,4}. The research interest of these oxides has been increased in the last few years due to their potential application in a wide variety of optical modulation devices⁵. The smart reversible MIT makes vanadium oxide a promising material for the various applications, e.g. intelligent energy conserving window coating⁶, infrared (IR) light switching or bolometric devices⁷, electrochromic devices^{6,7}, colour memory devices⁵ and variable emitting smart surface for spacecraft application^{8,9}.

Several techniques have been utilized to deposit vanadium oxide films such as sputtering¹⁰⁻¹⁴, pulsed laser deposition^{15,16}, thermal evaporation¹⁷⁻²⁰, electron beam evaporation²¹, spray pyrolysis^{22,23} and sol-gel²⁴⁻²⁶. However, sputtering technique is most advantageous than the other methods due to its high deposition rate and good uniformity¹³. The studies in systematic variation in RF power during sputtering of vanadium oxide and further detailed structural, thermo-optical and

electrical behaviours have not been reported yet in literature. Moreover, phase transition behaviour of vanadium oxide thin films/coatings has not been attempted so far in particular by calorimetric technique; although the phase transition behaviour of both VO_2 ²⁷ and V_2O_5 ^{28,29} either in powder form²⁷ or nanostructured powder dispersed in solution²⁸ has been studied. In addition, works related to mechanical properties of vanadium oxide films/coatings especially at microstructural length scale is scarce in literature and the reported hardness and Young's modulus values were unexpectedly scattered and ambiguous^{30,31}.

Hence, in the present work, development and systematic studies of vanadium oxide thin films have been attempted. Vanadium oxide films were deposited on quartz glass and Si(111) substrates by pulsed RF magnetron sputtering by varying RF power from 100 W to 700 W. Further, microstructure, electronic structure, phase transition behavior, electrical properties, thermo-optical, and nanomechanical properties were investigated in detail.

2. Materials and methods

Pulsed RF magnetron sputtering system (SD20, Scientific Vacuum Systems, UK) was utilized to deposit the vanadium oxide thin films on quartz glass and Si(111) substrates at room temperature. The quartz substrate (40 mm x 40 mm x 0.2 mm) was obtained from Astro Optics, India and boron doped p type Si(111) (diameter:125 mm and thickness:0.6 mm) was procured from Silicon Valley Microelectronics Inc., USA. The V_2O_5 target (99.999%, diameter: 200 mm and thickness: 3 mm, Vin Karola Instruments, USA) was used in the present case. The distance between the target and the substrate was kept as 140 mm. The RF power during the film deposition was varied from 100 W to 700 W with the constant increment of 100 W while the duration of deposition time was kept constant for 1 hr. The pulse frequency was 100 Hz with duty cycle of 57%. The vacuum chamber was evacuated to a pressure of 5×10^{-6} mbar prior to deposition utilizing combination of both rotary (i.e. roughing) and turbo molecular pumps. However, the working pressure was set as constant 1.5×10^{-2} mbar after introducing ultra pure argon gas. Pre-sputtering was carried out for 10 min prior to deposition of films to reduce the contamination.

Thickness of the deposited films were measured using a surface profilometer (Nanomap 500 LS 3D, USA). Phase analysis of the deposited films was investigated by the X-ray diffraction (XRD) technique using a commercial diffractometer (X'pert Pro, Philips, The Netherlands). The $\text{CuK}_{\alpha 1}$ radiation was used at a glancing incident angle of 2° with a very slow step size of 0.03° . The surface topography of the deposited thin films was observed by field emission scanning electron microscopy (FESEM: SupraVP35 Carl Zeiss, Germany). The energy dispersive X-ray (EDX: X-Max, USA) spectra of the deposited films were acquired utilizing a customary unit (Oxford Instruments, UK) attached to the FESEM. XPS of deposited films on silicon substrate were recorded with a SPECS spectrometer using non-monochromatic $\text{AlK}\alpha$ radiation (1486.6 eV) as an X-ray source run at 150 W (12 kV, 12.5 mA). The binding energies reported here were referenced with O1s peak at 530.0 eV³². All the survey spectra were obtained with pass energy of 70 eV with step increment of 0.5 eV, whereas individual spectra were recorded with pass energy and step increment of 25 and 0.05 eV, respectively. V2p–O1s core level spectra were curve fitted into their several components with Gaussian-Lorentzian peaks after Shirley background subtraction employing CasaXPS program.

Phase transition temperature of vanadium oxide films were investigated employing differential scanning calorimetry (DSC) technique (Q100, TA Instruments, USA) in helium environment. An average hemispherical emittance ($\epsilon_{\text{IR-H}}$) of the deposited vanadium oxide films was measured by an emissometer (AE, Devices and Services Co., USA.) in the wavelength range of 3 μm to 30 μm using both high and low emitting standard surfaces as per ASTM C1371–04a.

Sheet resistance (R_s) of deposited vanadium oxide films was measured by the two-probe resistance meter (Trek Model 152-1, Trek Inc., USA) as per ASTM D 257-9.

The optical properties of the vanadium oxide thin films deposited on quartz substrate were obtained by the UV–VIS–NIR spectrophotometer (Cary 5000, Agilent Technologies, USA) in the entire solar region (i.e. 200 nm to 2.5 μm) of the spectral window. Average solar absorptance (α_s) was evaluated by the solar spectrum reflectometer (SSR-E, Devices and Services Co., USA,) as per

ASTM C1549-09. The absorption coefficient (α) of the vanadium oxide films was calculated from the transmittance data received from UV-VIS-NIR spectrophotometer from the following relations (1 to 3). Further, 'Tauc extrapolation plot' was utilized to evaluate the optical band gap (E_0) of the deposited films. The ' α ' of the film can be represented by the following equation (1)^{33,34}:

$$\alpha h\nu = A(E_i - E_0)^m \quad (1)$$

where, E_0 and E_i are initial energy of the photon and energy of the incident photon, respectively while proportionality constant and Planck's constant are represented as A and h , respectively. The α and ν are known as absorption coefficient and frequency, respectively. The magnitude of ' m ' is 2, for indirect optical band gap, respectively³⁴. The quantities ' α ' and the total transmission (T) are correlated by the following relations (equation (2) to (3)):

$$T = e^{-\alpha t} \quad (2)$$

or

$$\alpha = (\ln T) / t \quad (3)$$

where, ' t ' is the thickness of the deposited film.

Finally, The nanomechanical properties e.g., nanohardness (H) and Young's modulus (E) of the vanadium oxide film was evaluated by nanoindentation (G200, MTS-Agilent technologies, USA) technique with continuous stiffness measurement (CSM) mode. The Berkovich diamond indenter with tip radius of ~ 20 nm was used in the present case. Thick (~ 3.8 μm) vanadium oxide coating deposited at RF power of 700 W on silicon substrate was judiciously utilized in the present nanoindentation study to avoid the substrate influence. Generally, the depth of penetration of the indenter which is $\sim 10\%$ of the film thickness is recommended during conducting nanoindentation experiment. The slackness can be attributed to the influence of the mechanical properties of the substrate as well³⁵ Therefore, to avoid the substrate's mechanical property, the final depth of penetration has been wisely chosen as 300 nm which is well below 10% of the film thickness (i.e.

~3.8 μm). Further, CSM mode was employed in the present study to investigate the depth dependence of the mechanical properties in the deposited vanadium oxide film, if any.

3. Results and discussion

The thicknesses of the deposited films measured by nanoprofilometric technique are 27.5 nm, 40 nm, 102 nm, 145 nm, 200 nm, 230 nm and 243 nm for quartz substrate and 21 nm, 36 nm, 89 nm, 133 nm, 156 nm, 201 nm, 156 nm and 211 nm for silicon substrate as increase in RF power from 100 W to 700 W with the constant increment of 100 W (Fig. 1). The increase in RF power leads to increase in deposition rate as the deposition duration is kept constant which ultimately results in increase in film thickness. Marginally lower thickness of deposited films is observed on silicon substrates than on quartz substrates.

All as-grown films are confirmed to be amorphous in nature by XRD analyses. RF sputtering technique often offers amorphous vanadium oxide film at room temperature deposition^{36,37}. Crystallinity can be achieved at elevated substrate temperature³⁸⁻⁴¹, post annealing^{36,40-43} and increase in oxygen partial pressure^{37,41}.

The FESEM photomicrographs of the thin films deposited on silicon substrate with thicknesses of 21 nm, 156 nm, and 211 nm grown at 100 W, 500 W and 700 W, respectively for constant duration of 1 hr. are shown in Fig. 2 (a-c), respectively. Featureless, smooth and compact surfaces are observed in Fig. 2 (a-c). The corresponding EDX spectra are appended in the insets of the Fig. 2 (a-c). The presence of only V and O are observed in the corresponding EDX spectra. However, the presence of substrate peak is also prominent as the thickness of the film is very less³⁴. The intensities of vanadium and oxygen peaks are increased as the thickness of the film increased as expected.

Figure 3a shows the typical XPS survey spectra of deposited vanadium oxide thin films grown on silicon substrates at 100 W and 600 W. It clearly shows the presence of V and O species in deposited films. Typical XPS of V2p core levels in vanadium oxide films deposited with different powers are shown in Fig. 3b. Both V2p and O1s core level spectra are kept together in the

Fig. 3b as V2p and O1s core level regions are nearby. No significant alteration of the characteristics peaks in terms of position and intensity are observed with the variation of RF power. Spectral envelopes of V2p core levels of as-grown films contain long tail in the lower binding energy region along with main peak indicating that V is present in different oxidation states and it can be curve-fitted into sets of spin-orbit doublets. Accordingly, observed V2p_{3/2} peaks at 516.2 and 517.2 eV in all films are assigned to V⁴⁺ (VO₂) and V⁵⁺ (V₂O₅) species. Three component peaks are fitted in O1s core level region (Fig. 3c). Component peak at 530.1 is associated with oxide species related to vanadium oxides, whereas peaks at 531.5 and 533.1 eV correspond to adsorbed oxygen and water, respectively present in the films.⁴⁴ Peak areas (A) of V⁵⁺ and V⁴⁺ components are used to estimate their relative concentrations (C) in the films using the following equation:

$$C_{V^{4+}} = \frac{A_{V^{4+}}}{A_{V^{5+}} + A_{V^{4+}}} \quad (4)$$

According to the equation (4), the concentration of V⁴⁺ in the film deposited with RF power of 100 W is estimated to be 20% with respect to the total amount of V species. Binding energies and relative surface concentrations of different V species as obtained from V2p core levels of vanadium oxide films grown at different RF powers are summarized in Table 1. It is observed from Table 1 that concentrations of V⁴⁺ species are in the range of 18% to 25% with remaining of V⁵⁺ species. It is to be noted that the characteristic binding energies of V2p_{3/2} core level peaks for V²⁺, V³⁺, V⁴⁺ and V⁵⁺ are reported as 513.5-513.7 eV^{45,46-48}, 515.15-515.7 eV^{45,48-51}, 515.8-516.2 eV^{45,48-51} and 516.9-517.3 eV^{45,49-51}, respectively. In the present study, fitted curves clearly show that the characteristic peaks corresponds to the V⁴⁺ and V⁵⁺ possessing binding energies of V2p_{3/2} as 516.1-516.2 eV and 517.1-517.3 eV, respectively (Table 1).

Present XPS data demonstrate that there is insignificant variation in the electronic structure and oxidation state of vanadium oxide as an alteration of RF power. Further, pure phase of V₂O₅ and VO₂ developed by sputtering technique in particular are seldom reported in the literature^{42,52}. In general, sputtered vanadium oxide films showed mixed phases with one or more vanadium species

that includes VO_2 , V_2O_5 , V_3O_7 , V_4O_7 , and V_6O_{13} ^{53,54}. However, in the present study, no other V species was found except V^{4+} and V^{5+} .

The variation of derived heat flow of bare quartz and vanadium oxide thin films grown with 100 W-700 W on quartz glass as a function of temperature is shown in Fig. 4 to investigate phase transition of present vanadium oxide films. Both in heating and cooling cycles, any signature of phase transition is not observed in bare quartz glass as expected. However, vanadium oxide thin films show prominent peaks appeared in both heating and cooling cycles around in the region from 337 °C to 343 °C which indicates the phase transition temperature. Further, in both heating and cooling cycles, the curves of derived heat flow follow almost same path which implies that the hysteresis loss is insignificant and proves the reversible or smart characteristic transition. In the present case, the transition temperatures are almost remaining constant despite the increase in RF power. In other word, phase transition temperatures of vanadium oxide films are insignificantly varied as function of RF power. This observation is corroborated with the XPS investigation where it has been seen that the oxidation state of vanadium oxide is insignificantly altered as increase in RF power summarized in Table 1.

DSC studies of V_2O_5 thin films are not yet reported in literature. However, DSC investigation of nano-structured V_2O_5 powder via thermal decomposition of vanadyl oxalate ($\text{VOC}_2\text{O}_4 \cdot n\text{H}_2\text{O}$) indicates that the phase transition occurred in the range of 267°C to 353°C which gives an endothermic peak²⁸. Three exothermic peaks at 183°C, 261°C and 418°C are observed which attribute to evaporation of the absorbed organic compounds on the V_2O_5 foam surface, decomposition of the organic molecules (e.g. hexadecylamine) intercalated among the V_2O_5 layers and recrystallization of the V_2O_5 foam, respectively²⁹. The phase transition of $\beta\text{-V}_2\text{O}_5$ powder heated in an oxygen atmosphere is reported in the range of 220 °C to 425 °C studied through DSC⁵⁵. V_2O_5 nanobelt grown by xerogel process show a transition at ~465.6 °C measured by DSC technique⁵⁶. Further, V_2O_5 powder and dissolved V_2O_5 powder in H_2O_2 show transition in the range of 239 °C to 344°C⁵⁷ and 357°C⁵⁸, respectively. Hence, aforesaid DSC studies on powder V_2O_5

samples reveal that the range of transition temperature of V_2O_5 is widely scattered and depends on the processing technique of V_2O_5 as well as its phase purity.

The variation of ϵ_{IR-H} (using both high and low emitting standard surfaces) of the vanadium oxide thin films on quartz glass substrate as a function of RF power is shown in Fig. 5. The ϵ_{IR-H} data of bare quartz is around 0.78 which is not significantly altered after coated with vanadium oxide. Further, no significant change in ϵ_{IR-H} has been observed when it is measured with low or high emitting standard surface. This data depict that the deposited vanadium oxide is transparent in IR region that agrees well with literature⁵⁹.

Further, variation of R_s values is insignificantly altered as increase in RF power. The values of R_s are in the range of 10^6 to 10^5 Ω /square which agrees well with the R_s data reported for vanadium oxide films⁶⁰.

The solar transmittance spectra of different vanadium oxide thin films deposited on quartz substrate at 100 W to 700 W as a function of wavelength in entire solar regime of the spectral window are shown in Fig. 6a. Further, transmittance spectra shown in Fig. 6a are further blown up and shown in Fig. 6b, c and d for ultra violet (UV: 200-340 nm), visible (VIS: 340-780 nm) and near infrared (NIR: 780-2300 nm) region, respectively. The bare quartz glass shows almost 94% constant transmittance value. The transmittance of vanadium oxide film decreases as the thickness of the film increases from 27.5 nm to 243 nm due to increase in RF power. In UV regime, transmittance decreases considerably from ~75% to ~1%. In VIS regime, similar trend is also observed, however the transmittance value is not constant throughout the VIS regime. Further, corresponding reflectance spectra are shown in Fig. 7. The reflectance is found to increase with increase in thickness of the film in particular at NIR regime except the film deposited at 700 W.

The decrement of average transmittance value at NIR regime is observed from ~0.2% to ~30% while thickness of the film increases only from 27.5 nm to 243 nm (Fig. 8a). The variation of α_s as a function of RF power is shown in Fig. 8b. The increase in α_s is observed with increase in thickness of the film as expected. The phenomenon of decrease in transmittance with increase in

thickness of vanadium oxide films while reverse trend observe for reflectance is well studied in literature^{61,62}. In the present work, significant decrease in transmittance is observed both in UV, VIS and NIR regions as increase in thickness which is only in nanometric range i.e., from ~27.5 nm to 243 nm. Thus, tuning of the transmittance of vanadium oxide film can be achieved for desired application only by altering thickness without tradeoff its structural phase, electronic configuration, and phase transition behaviour as well.

Further, variation of α as a function of photon energy calculated for indirect optical band gap is shown in Fig. 9. The optical band gap can be represented by the value of energy for which α is equal to zero. Thus, the linear portions of the corresponding absorption coefficient data plot (Fig. 9) are extrapolated to intersect the energy axes (i.e. 'x' axis) at $\alpha=0$. The corresponding values of the energy data give the optical band gap of the vanadium oxide film. The indirect optical band gap of vanadium oxide films grown at 100-700 W are summarized in Table 2. The optical band gap data is in the range of 2.2 eV to 2.8 eV. The present optical band gap data agree well with the data reported in the literature⁶³.

The variations of H and E as a function of depth are shown in Fig. 10 (a-b), respectively. Both H and E values are almost constant as ~0.2 GPa and 8.5 GPa, respectively. The large variation of both hardness and modulus of vanadium oxide films are reported in literature^{30,31}. For instance, with increase in deposition temperature, the V₂O₅ films by DC sputtering show a transition from amorphous at room temperature to polycrystalline growth with a preferred (200) orientation as demonstrated by Fateh and coworkers³⁰. This phenomenon leads to an increase in H and E values of the films from 3.2 ± 0.1 GPa and 79.4 ± 3.2 GPa at 26 °C to 4.8 ± 0.6 GPa and 129.2 ± 6.4 GPa at 300 °C, respectively. Further, Zhu et al. show ambiguous variation of E value of as-grown V₂O₅ nanobelts between 5.6 to 98 GPa³¹. They opine that such scattered values are attributed to the different contents of water molecules in the nanobelts. However, after annealing in vacuum, the nanobelts are converted to polycrystalline α -V₂O₅ phase which show consistent values of modulus as ~28.9 GPa. Thus, it is clearly observed that both hardness and modulus values of vanadium oxide

films depend upon crystallinity, growth axis and annealing temperature^{30,31}. In the present study, comparatively lower end data of hardness and modulus are found possibly due to lack of crystallinity of the vanadium oxide films as discussed earlier. Further, it is important to note that measured nanoindentation data depict that both hardness and modulus values are insignificantly varied as a function of depth.

4. Conclusions

Pulsed RF magnetron sputtering technique was utilized to grow amorphous, featureless and dense vanadium oxide thin films on both quartz glass and silicon substrates varying RF power from 100 W to 700 W with a thickness in the range of ~21 nm to ~243 nm. The deposited films show only the major presence of V⁵⁺ (75-82%) and minor presence of V⁴⁺ (18-25%) and no any other species of vanadium. The reversible i.e. smart transition of vanadium oxide films is observed in the temperature range of 337°C to 343°C. Present XPS data depict that there is insignificant variation in its electronic structure and vanadium oxidation states as an alteration of RF power and further DSC results also support the same. The hemispherical IR emittance of the quartz glass is not altered after deposition of vanadium oxide. Further, sheet resistance value of the vanadium oxide films is found in the range of 10⁶ to 10⁵ Ω/square. The significant decrease in solar transmittance and increase in solar absorptance of vanadium oxide films is observed while increase in thickness from 27.5 nm to 243 nm. The optical band gap of vanadium oxide films is found in the range from 2.2 eV to 2.8 eV. Finally, comparatively lower nanohardness and modulus values of vanadium oxide are measured as ~0.2 GPa and 8.5 GPa, respectively which plausibly due to the lack of crystallinity of the deposited vanadium oxide films. In addition, the present nanohardness and modulus data show almost depth independency behaviour.

References

- 1 N. F. Mott, *Rev. Mod. Phys.*, 1968, 40, 677.
- 2 S. N. Mott, *Phys. Today*, 1978, 31.
- 3 P. Kiri, G. Hyett and R. Binions, *Adv. Mater. Lett.*, 2010, 1, 86.
- 4 A. L. Pergament, G. B. Stefanovich, N. A. Kuldin and A. A. Velichko, *ISRN Cond. Matter Phys.*, 2013, 960627.
- 5 L. J. Meng, R. A. Silva, H. N. Cui, V. Teixeira, M. P. dos Santos and Z. Xu, *Thin Solid Films*, 2006, 515, 195.
- 6 M. A. Sobhan, M. R. Islam and K. A. Khan, *Appl. Energy*, 1999, 64, 345.
- 7 R. Mustafa Oksuzoglu, P. Bilgiç, M. Yildirim and O. Deniz, *Optic. Laser Technol.*, 2013, 48, 102.
- 8 R. V. Druzelecky, E. Haddad, W. Jamroz, M. Soltani and M. Chaker, Proceeding of 2003 SAE Conference, 2003-01-2472, Vancouver, BC, Canada, 2003.
- 9 M. Benkahoul, M. Chaker, J. Margot, E. Haddad, R. Kruzelecky, B. Wong, W. Jamroz and P. Poinas, *Sol. Energ. Mat. Sol. C.*, 2011, 95, 3504.
- 10 X. Chen and J. Dai, *Optik – Int. J. Light Elec. Optic.*, 2010, 121, 1529.
- 11 Q. Jiang, Y. Li, S. Hu, B. Wu, X. Yu and H. Wang, Proceeding of SPIE 7279, Photonics and Optoelectronics Meetings POEM 2008: Optoelectronic Devices and Integration, 2009.
- 12 E. Cazzanelli, G. Mariotto, S. Passerini, W. H. Smyrl and A. Gorenstein, *Sol. Energ. Mat. Sol. C.*, 1999, 56, 249.
- 13 M. Jiang, X. Cao, S. Bao, H. Zhou and P. Jin, *Thin Solid Films*, 2014, 562, 314.
- 14 Y. Lv, M. Hu, M. Wu and Z. Liu, *Surf. Coat. Technol.*, 2007, 201, 4969.
- 15 C. V. Ramana, R. J. Smith, O.M. Hussain, M. Massot and C. M. Julien, *Surf. Interface Anal.*, 37 2005 406.
- 16 M. Maaza, K. Bouziane, J. Maritz, D. S. McLachlan, R. Swanepool, J.M. Frigerio and M. Every, *Optic. Mater.*, 2000, 15, 41.

- 17 R. Santos, J. Loureiro, A. Nogueira, E. Elangovan, J. V. Pinto, J. P. Veiga, T. Busani, E. Fortunato, R. Martins and I. Ferreira, *Appl. Surf. Sci.*, 2013, 282, 590.
- 18 L. Derbali and H. Ezzaouia, *Sol. Energy*, 2012, 86, 1504.
- 19 X. Wu, F. Lai, L. Lin, Y. Li, L. Lin, Y. Qu and Z. Huang, *Appl. Surf. Sci.*, 2008, 255, 2840.
- 20 A. Axelevitch, B. Gorenstein and G. Golan, *Microelectron. Reliab.*, 2011, 51, 2119.
- 21 C. V. Ramana, O. M. Hussain, B. Srinivasulu Naidu, C. Julien and M. Balkanski, *Mater. Sci. Eng. B*, 1998, 52, 32.
- 22 A. Ashour and N. Z. El-Sayed, *J. Optoelectron. Adv. Mater.*, 2009, 11, 251.
- 23 A. Bouzidi, N. Benramdane, S. Bresson, C. Mathieu, R. Desfeux and M.E. Marssi, *Vib. Spectros.*, 2011, 57, 182.
- 24 D. Q. Liu, W. W. Zheng, H. F. Cheng and H. T. Liu, *Adv. Mater. Res.*, 2009, 79-82, 747.
- 25 J. Wu, W. Huang, Q. Shi, J. Cai, D. Zhao, Y. Zhang and J. Yan, *Appl. Surf. Sci.*, 2013, 268, 556.
- 26 H. K. Chen, H. C. Hung, T. C. K. Yang and S. F. Wang, *J. Non-Cryst. Solid.*, 2004, 347, 138.
- 27 Y. Zhang, M. Fan, M. Zhou, C. Huang, C. Chen, Y. Cao, G. Xie, H. Li and X. Liu, *Bull. Mater. Sci.*, 2012, 35, 369.
- 28 A. Pan, J. G. Zhang, Z. Nie, G. Cao, B. W. Arey, G. Li, S. Q. Liang and J. Liu, *J. Mater. Chem.*, 2010, 20, 9193.
- 29 C. H. Kim, Y. J. Yun, B. H. Kim, W. G. Hong, Y. Y. Kim, W. L. Jang, N. E. Lee and H. Y. Yu, *J. Nanomater.*, 2013, 807895.
- 30 N. Fateh, G. A. Fontalvo and C. Mitterer, *J. Phys. D Appl. Phys.*, 2007, 40, 7716.
- 31 Y. Zhu, Y. Zhang, L. Dai, F. C. Cheong, V. Tan, C. H. Sow and C. T. Lim, *Acta Mater.*, 2010, 58, 415.
- 32 G. Silversmit, D. Depla, H. Poelman, G. B. Marin and R. De Gryse, *Surf. Sci.*, 2006, 600, 3512.

- 33 P. Kumar, M. K. Wiedmann, C. H. Winter and I. Avrutsky, *Appl. Optic.*, 2009, 48, 5407.
- 34 I. N. Reddy, V. R. Reddy, N. Sridhara, V. S. Rao, M. Bhattacharya, P. Bandyopadhyay, S. Basavaraja, A. K. Mukhopadhyay, A. K. Sharma and A. Dey, *Ceram. Int.*, 2014, 40, 9571.
- 35 E. Uchaker, Y. Z. Zheng, S. Li, S. L. Candelaria, S. Hu and G. Z. Cao, *J. Mater. Chem. A*, 2014, 2, 18208.
- 36 C. R. Cho, S. Cho, S. Vadim, R. Jung and I. Yoo, *Thin Solid Films*, 2006, 495, 375.
- 37 M. Benmoussa, E. Ibnouelghazi, A. Bennouna and E. L. Ameziane, *Thin Solid Films*, 1995, 265, 22.
- 38 S. C. Mui, J. Jasinski, V. J. Leppert, M. Mitome, D. R. Sadoway and A. M. Mayes, *J. Electrochem. Soc.*, 2006, 153, A 1372.
- 39 S. Saitzek, F. Guinneton, G. Guirleo, L. Sauques, K. Aguir and J.-R. Gavarri, *Thin Solid Films*, 2008, 516, 891.
- 40 Y. Zhang, R. Wang, Z. Qiu, X. Wu and Y. Li, *Mater. Lett.*, 2014, 131, 42.
- 41 J. W. Lee, S. R. Min, H. N. Cho and C. W. Chung, *Thin Solid Films*, 2007, 515, 7740.
- 42 A. A. Akl, *Appl. Surf. Sci.*, 2007, 253, 7094.
- 43 M. I. Kang, I. K. Kim, E. J. Oh, S. W. Kim, J. W. Ryu and H. Y. Park, *Thin Solid Films*, 2012, 520, 2368.
- 44 J. Liqiang, W. Baiqi, X. Baifu, L. Shudan, S. Keying, C. Weimin and F. Honggang, *J. Solid State Chem.*, 2004, 177, 4221,
- 45 N. Alov, D. Kutsko, I. Spirovová and Z. Bastl, *Surf. Sci.*, 2006, 600, 1628.
- 46 M. D. Negra, M. Sambì and G. Granozzi, *Surf. Sci.*, 1999, 436, 227.
- 47 M. Petukhov, G. A. Rizzi and G. Granozzi, *Surf. Sci.*, 2001, 490, 376.
- 48 G. Silversmit, D. Depla, H. Poelman, G. B. Marin and R. De Gryse, *J. Electron. Spectrosc.*, 2004, 135, 167.
- 49 J. Mendiàdua, R. Casanova and Y. Barbaux, *J. Electron. Spectrosc.*, 1995, 71, 249.
- 50 G. A. Sawatzky and D. Post, *Phys. Rev. B*, 1979, 20, 1546.

- 51 M. Demeter, M. Neumann and W. Reichelt, *Surf. Sci.*, 2000, 454–456, 41.
- 52 M. Jiang, X. Cao, S. Bao, H. Zhou and P. Jin, *Thin Solid Films*, 2014, 562, 314.
- 53 C. Batista, V. Teixeira and J. Carneiro, *J. Nano Res.*, 2008, 2, 21.
- 54 C. Liu, M. P. Jiang, J. H. Li and S. K. Wang, *Adv. Mater. Res.*, 2011, 399-401, 589.
- 55 S. Ji, Y. Zhao, F. Zhang and P. Jin, *J. Ceram. Soc. Jap.*, 2010, 118, 867.
- 56 C. V. S. Reddy, J. Wei, Z. Quan-Yao, D. Zhi-Rong, C. Wen, S. Mho and R. R. Kalluru, *J. Power Sources*, 2007, 166, 244.
- 57 V. B. Chanshetty, K. Sangshetty and G. Sharanappa, *Int. J. Eng. Res. Appl.*, 2012, 2, 611.
- 58 F. P. Gokdemir, U. D. Menda, P. Kavak, A. E. Saatci, O. Ozdemir and K. Kutlu, *Proc. AIP Conf.*, 2012, 1476, 279.
- 59 L. Jacques, *Coordin. Chem. Rev.*, 1999, 190-192, 391.
- 60 K. Karsli, Dissertation: Middle East Technical University, Ankara, Turkey, 2012.
- 61 N. R. Mlyuka, G. A. Niklasson and C. G. Granqvist, *Sol. Energy Mater. Sol. Cells*, 2009, 93, 1685.
- 62 F. Guinneton, L. Sauques, J. C. Valmalette, F. Cros and J. R. Gavarrri, *Thin Solid Films*, 2004, 446, 287.
- 63 Z. Luo, Z. Wu, T. Wang, X. Xu, W. Li, W. Li and Y. Jiang, *J. Phys. Chem. Solid.*, 2012, 73, 1122.

Figure Captions

Figure 1: The variation of deposited film thicknesses on quartz and Si(111) substrates as a function of RF power.

Figure 2: Typical FESEM photomicrographs of vanadium oxide thin films grown on silicon substrate at different RF power e.g., (a) 100W, (b) 500 W and (c) 700 W. (Insets: corresponding EDX spectra).

Figure 3: (a) Typical XPS survey spectra of vanadium oxide thin films deposited at RF power of 100 W and 600 W. (b) V2p and O1s core level spectra of vanadium oxide thin films deposited with different RF power. (c) Typical curve-fitted V2p and O1s core level spectrum of vanadium oxide thin film deposited at 600 W.

Figure 4: The variation of derived heat flow of bare quartz and vanadium oxide thin films on quartz as a function of temperature.

Figure 5: The variation of average hemispherical emittance ($\epsilon_{\text{IR-H}}$) of the vanadium oxide thin films on quartz substrate as a function of RF power.

Figure 6: (a) The transmittance spectra of vanadium oxide thin film on quartz substrate at 200-2300 nm of the spectral window, blown up view of Fig. 5a: (b) UV region (200-340 nm), (c) VIS region (340-780 nm) and (d) NIR region (780-2300 nm).

Figure 7: The reflectance spectra recorded in 200-2300 nm of the spectral window for vanadium oxide thin films deposited on quartz surface at 100-700 W.

Figure 8: (a) Average transmittance in NIR region with respect to bare quartz. (b) Average solar absorptance (α_s) of vanadium oxide thin films coated on quartz as a function of RF power.

Figure 9: The variation of absorption coefficient (α) as a function of photon energy of vanadium oxide film on quartz substrate developed at 700 W for calculation of indirect optical band gaps.

Figure 10: (a) Nanohardness and (b) modulus of vanadium oxide film as a function of depth.

Table Captions

Table 1: Binding energies and relative peak areas of V species evaluated from XPS studies for the vanadium oxide thin films.

Table 2: Indirect optical band gap of vanadium oxide thin films.

Table 1

RF power (W)	V species	Binding energy of V2p _{3/2} (eV)	Relative peak area (%)
100	V ⁴⁺	516.1	20
	V ⁵⁺	517.1	80
200	V ⁴⁺	516.1	18
	V ⁵⁺	517.2	82
300	V ⁴⁺	516.1	25
	V ⁵⁺	517.3	75
400	V ⁴⁺	516.0	25
	V ⁵⁺	517.2	75
500	V ⁴⁺	516.0	25
	V ⁵⁺	517.3	75
600	V ⁴⁺	516.2	20
	V ⁵⁺	517.2	80
700	V ⁴⁺	516.1	25
	V ⁵⁺	517.1	75

Table 2

RF power (W)	Optical band gap (eV)
100	2.8
200	2.4
300	2.4
400	2.6
500	2.5
600	2.6
700	2.6

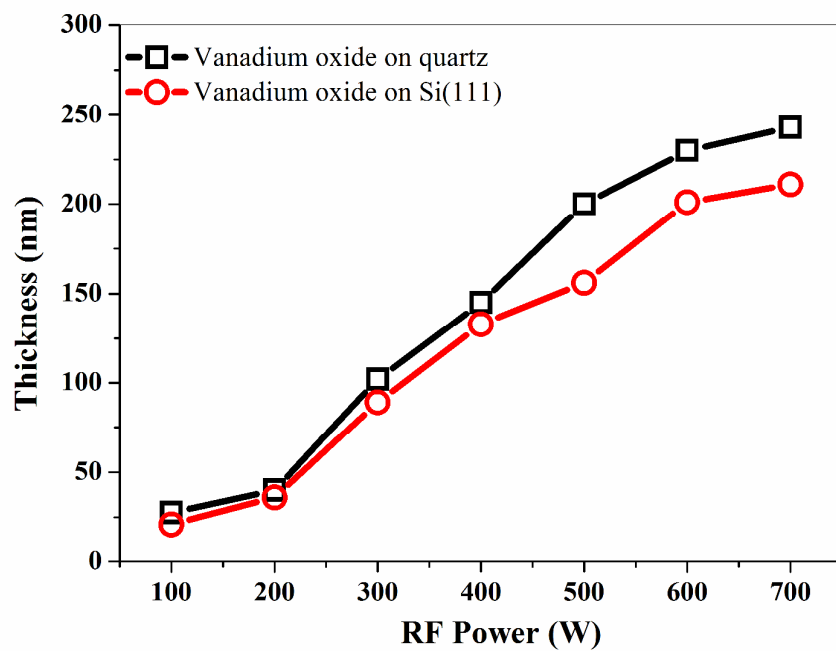


Fig. 1

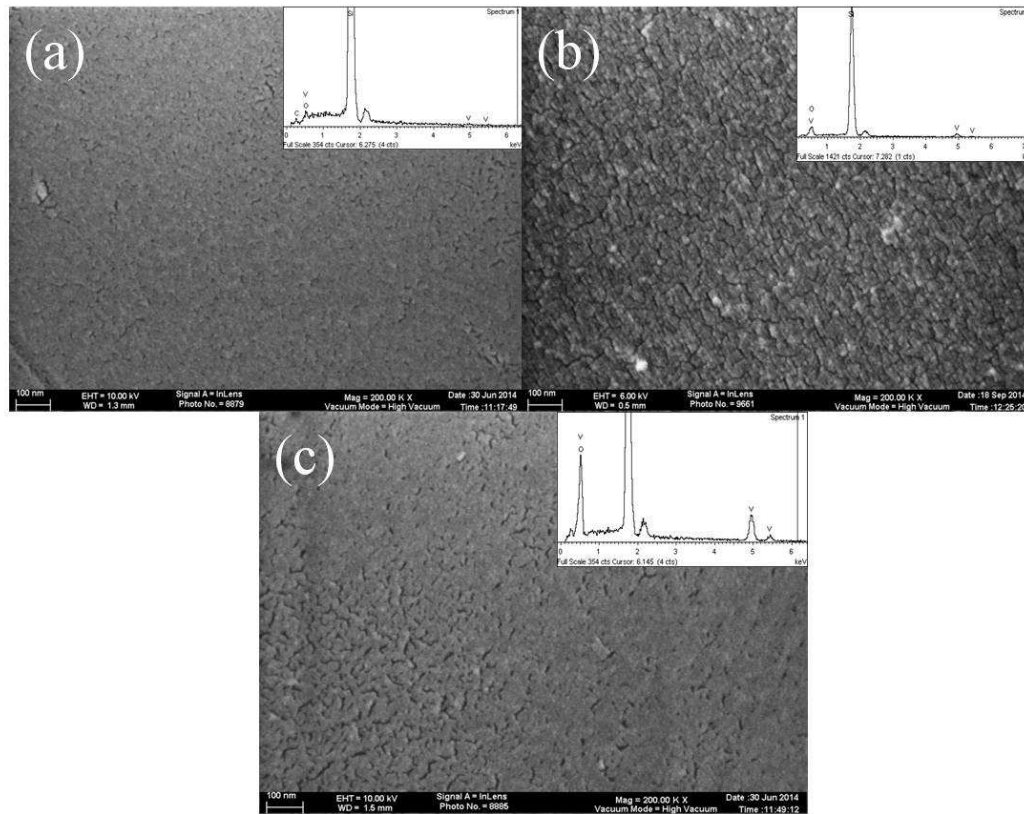


Fig. 2 (a-c)

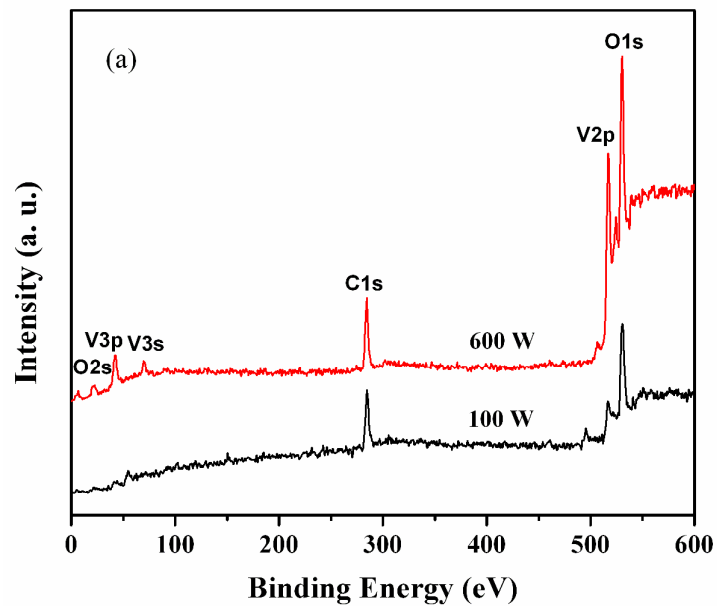


Fig. 3a

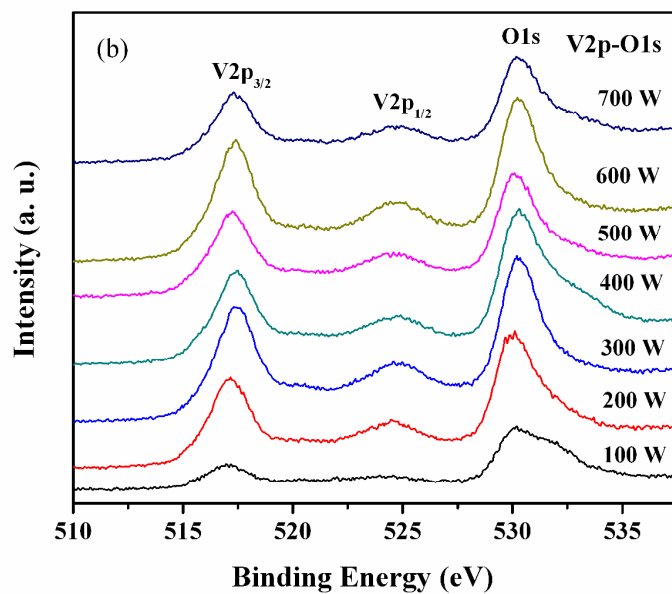


Fig. 3b

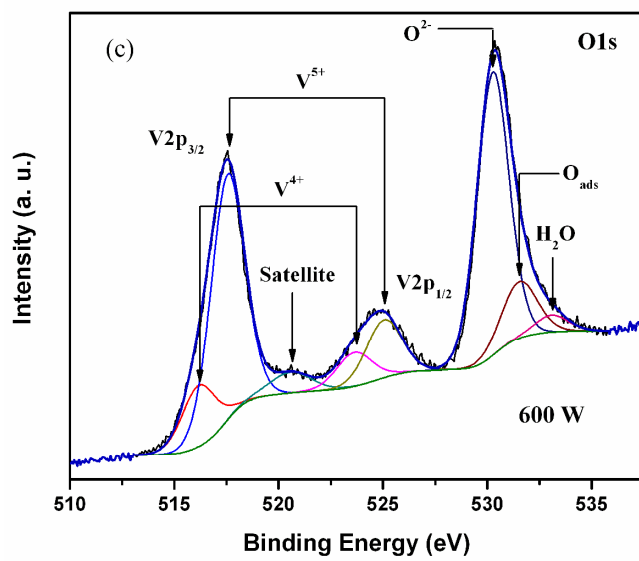


Fig. 3c

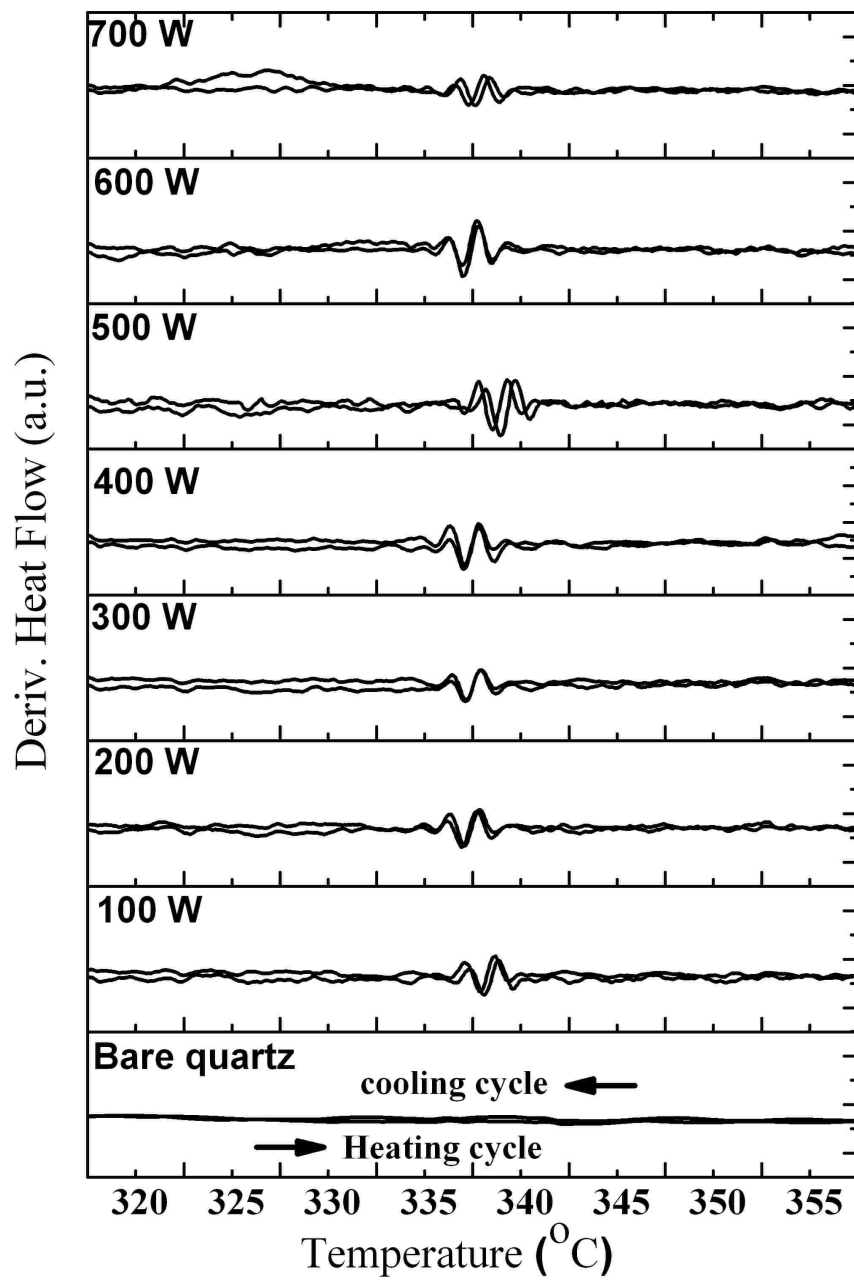


Fig. 4

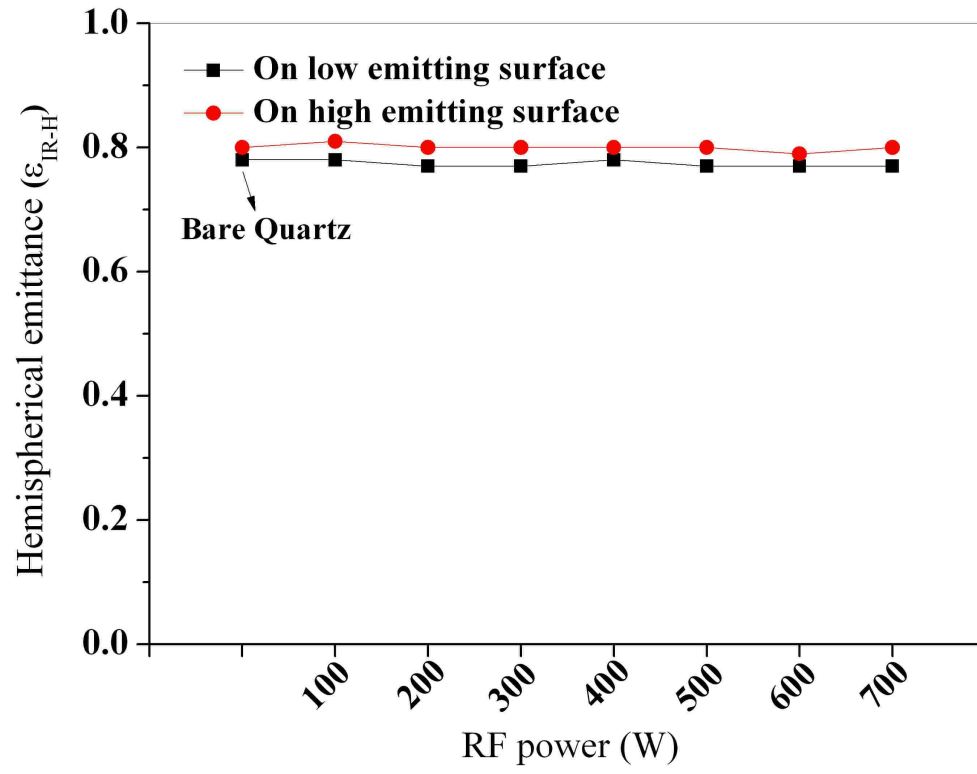


Fig 5

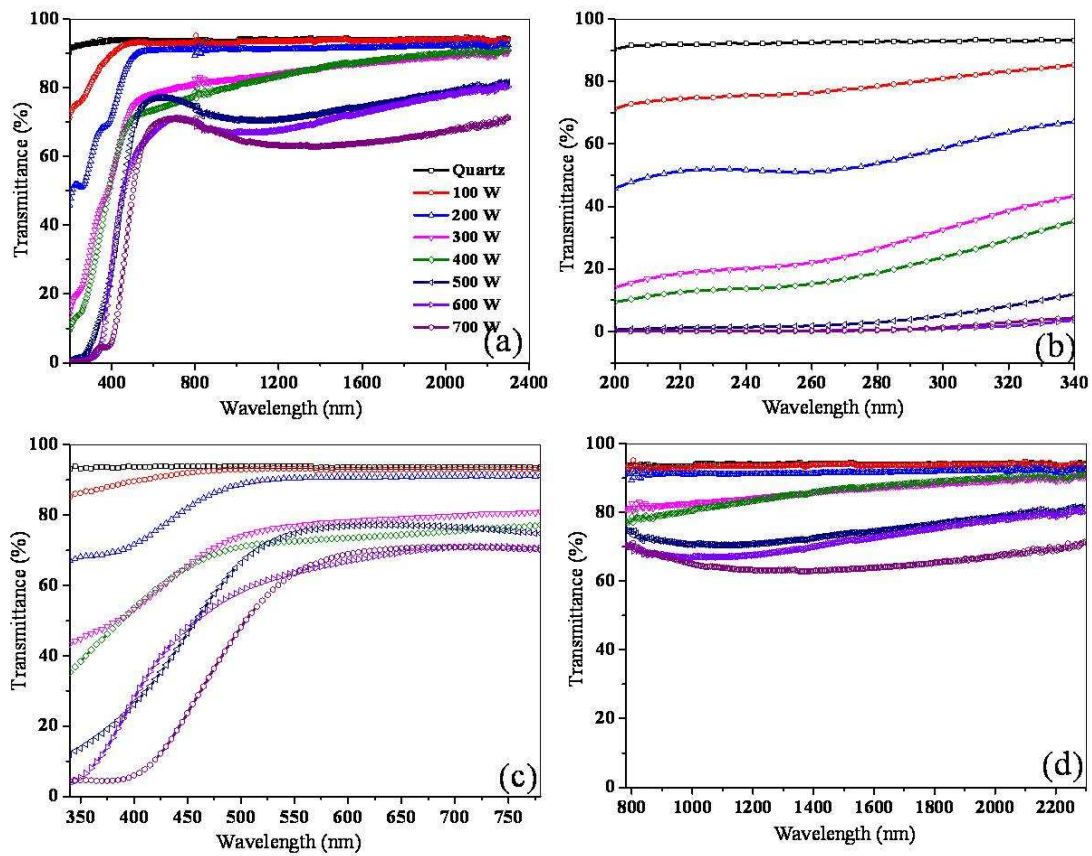


Fig 6

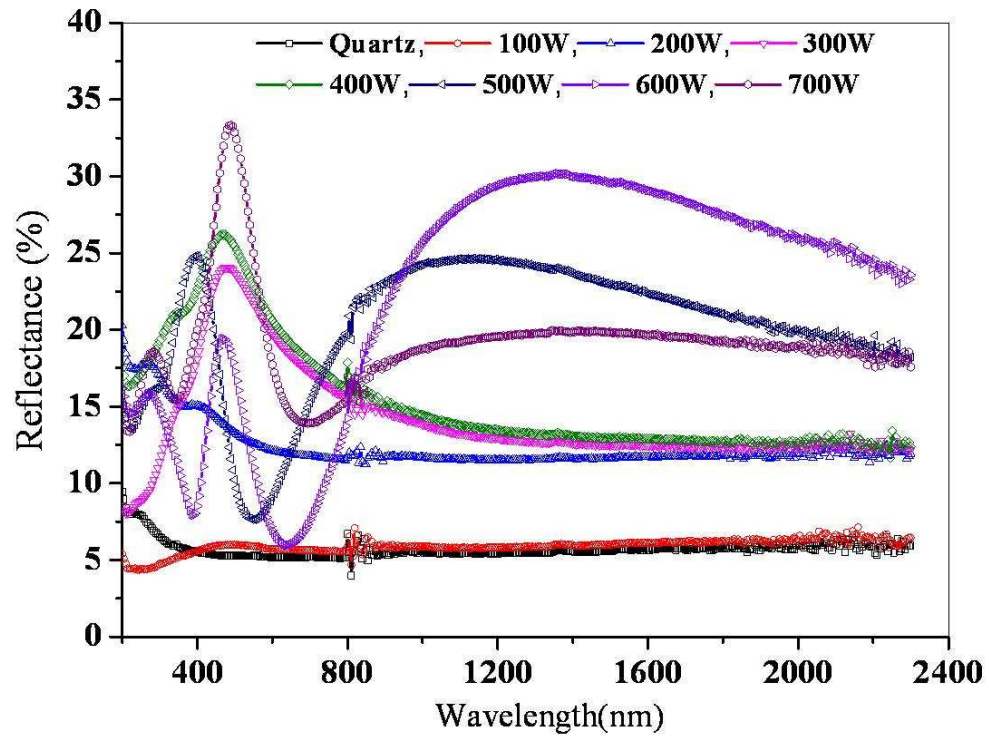


Fig. 7

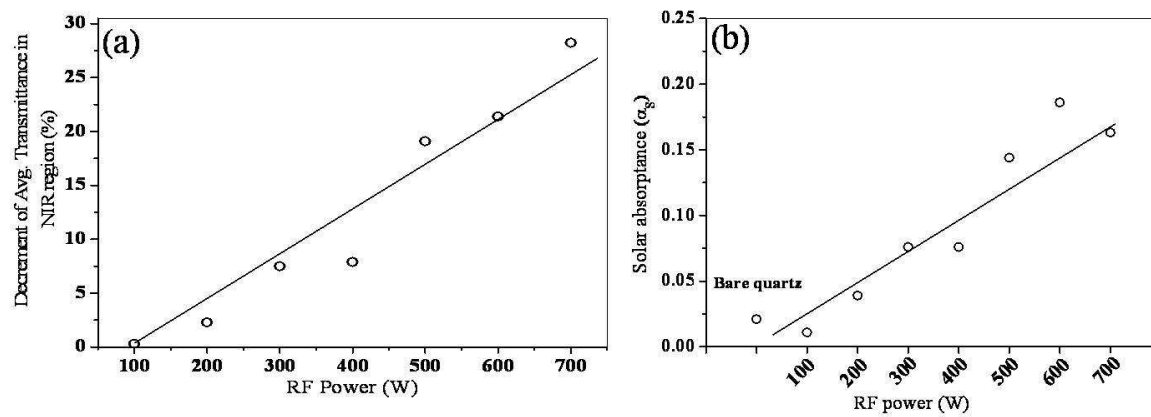
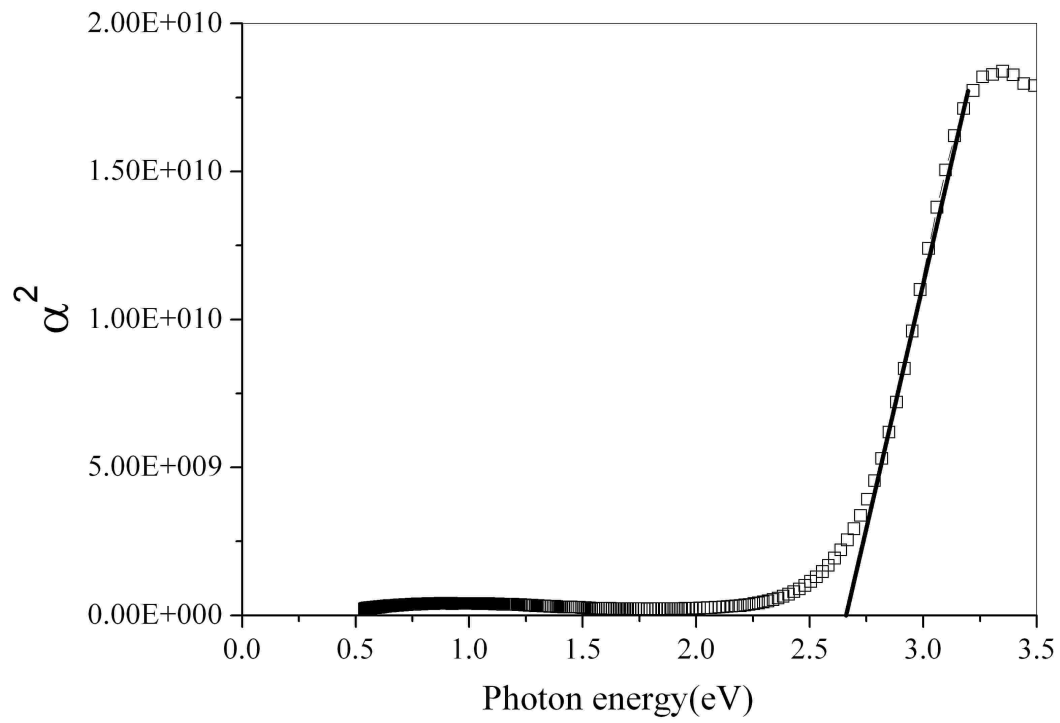


Fig. 8(a-b)

**Fig 9**

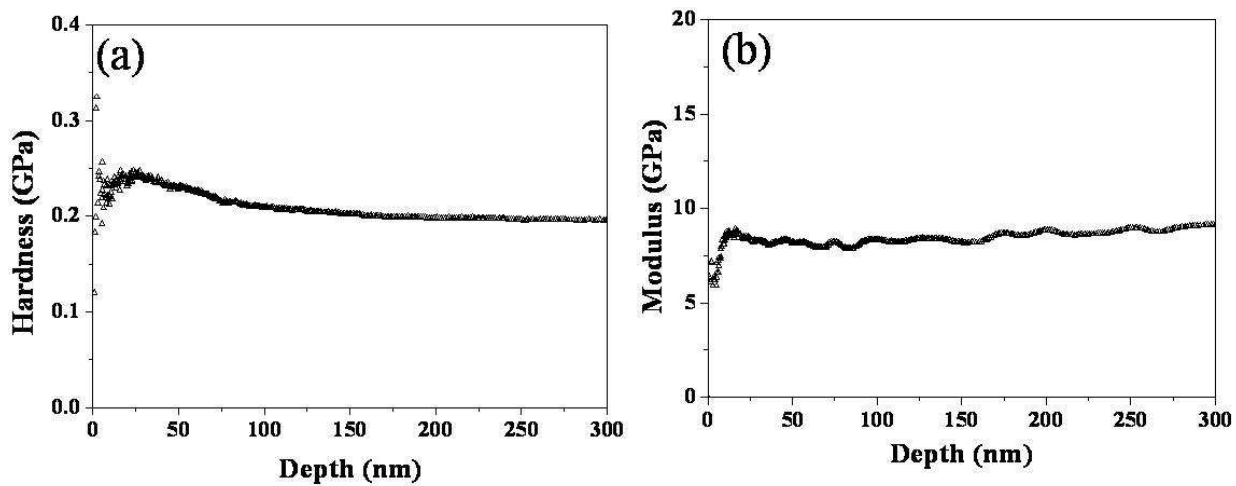


Fig 10 (a, b)